lation (the continuous line) with the results of experiments (we assumed in the calculations that μ_p = 270 kg/mm^2, and μ_t = 960 kg/mm^2). Comparison shows that there is quite satisfactory agreement between the experimental and theoretical data.

The author thanks E. I. Shemyakin and R. Kh. Izmagilov for their help in carrying out this work.

LITERATURE CITED

1. S. A. Khristianovich and E. I. Shemyakin, "Plane deformation of a plastic material for complex loading," Izv. Akad. Nauk SSSR, Mekh. Tverd. Tela., No. 9 (1969).
2. P. M. Naghdi and I. C. Rowley, "An experimental study of biaxial stress–strain relations in plasticity," J. Mech. Phys. Solids, 3 (1954).
3. S. A. Kristianovich and E. I. Shemyakin, "The theory of ideal plasticity," Inzh. Zh. Mekh. Tverd. Tela., No. 4 (1967).
4. S. A. Khristianovich, "Deformation of a strengthened plastic material," Izv. Akad. Nauk SSSR, Mekh. Tverd. Tela., No. 2 (1974).

MOBILE LOAD ON A LAYER OF IDEALLY PACKED MATERIAL

I. V. Simonov

UDC 539.374

1. Physical Assumptions. A plane load, the shape and value of which does not change with time, moves with constant velocity U_0 over the external surface of a layer of material of constant thickness h, lying without friction on a rigid base. We will study the plane stationary motion of the medium when a shockwave $U_0 > D_0$ exists, where D_0 is the wave velocity of the corresponding pressure P_{00}, in a system of coordinate (x, y) (Fig. 1), connected with the moving load $P_0(x)$ ($P_0(x) = 0$, $x > 0$, $P_0(0) = P_{00}$). Before the wavefront the medium is unperturbed: $P = 0$, $U = 0$, $\rho = \rho_0$ (P is the pressure, U is the mass velocity vector in the fixed system of coordinates, and ρ, ρ_0 is the current and initial density).

The material satisfies the barotropic equation of state. Its $P - \theta$ characteristic is shown in Fig. 2 (the continuous line). The equation of the straight line KM is $dP/d\rho = c^2 = \text{const}$ when $P(\theta_0) = P_{00}$ ($\theta = (\rho - \rho_0)/\rho_0$ is the volume deformation). This scheme is an idealization of the actual behavior of materials containing cavities or pores filled with easily compressed material (the dashed line in Fig. 2). The initial nonlinear part of the loading can sometimes be neglected when the characteristic pressure is higher than the pressure for which the pores collapse, and a further increment in the deformation occurs due to deformation of the matrix (for example, when the material is subjected to shock loading of considerable strength). For soft metals this region is from tens to several hundreds of kilobars. In this case the volume deformations of the matrix may remain small. For many materials the porosity is not reestablished when the load is removed, and it is possible to assume that the deformation is linear-elastic when the load is removed. Since the level of tangential stresses (determined by the relaxed amplitude of the elastic characteristic or limiting flow) is much less than the pressure of total packing, the resistance to shear can be neglected.

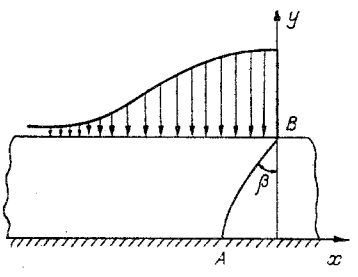

Fig. 1

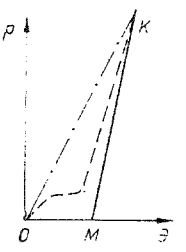

Fig. 2

Moscow. Translated from Zhurnal Prikladnoi Mekhaniki i Tekhnicheskoi Fiziki, No. 4, pp. 145-155, July-August, 1979. Original article submitted June 13, 1978.

Depending on the relation between U_0 and c we will have qualitatively different modes of reflection of an inclined shockwave from a rigid wall. When $U_0 > c$ regular reflection occurs with a series of alternating loading and unloading waves reflected from the external surface and the rigid wall. In this case regions of negative pressure may be formed in the material.

In this paper we will confine ourselves to investigating the mode in which $D_0 < U_0 < c$. In this case, like reflected waves, there will be no surface of discontinuity. Disturbances of a similar type, if they exist as an initial condition, overtake the leading edge and do not exist in the steady-state mode. Mathematically this is due to the fact that the equations become elliptic in the perturbed region.

The transient mode $U_0 \approx c$ will not be considered. As $U_0 \to c - 0$ the reflected wave fronts become vertical, and their intensity approaches infinity if the calculations are carried out within the framework of the scheme assumed. To eliminate this singularity it is necessary to take into account the nonlinear properties of the material and the convective terms in the equations of motion as in the theory of short waves.

The problem of the actual value of the interval (D_0, c) is important. For continuous materials and weak shock waves these quantities are close to one another. Qualitatively, the value of D_0 is determined by the slope of the line OK (Fig. 2), while the velocity of sound is given by the slope of KM, and hence even in the case of weakly porous materials they may differ considerably in value. For example, for an initial porosity of iron of 0.26 and pressures of ≈40-45 kbar on the shockwave front (the porosity becomes practically zero) $D \approx 1.65$-1.8 km/sec, while the velocity of sound in the dense iron powder is 4.6 km/sec [1] (there is unfortunately no data for smaller values of the porosity).

Note that for nonstationary and irregular (Mach) reflection of shockwaves, three shock waves exist starting from the same point. In the process we are investigating there is only a single shock wave, namely, a reflected wave which has, as it were, gone outside the limits of the region.

2. Mathematical Formulation. In the $\mathbf{x} = (x, y)$ plane we will consider a region Ω bounded by the straight lines $y = 0, h$, and an unknown continuous line $x = s(y)$, $y \in [0, h]$. The required functions $P(\mathbf{x})$, $\mathbf{U}(\mathbf{x}) = (U, V)$, $\rho(\mathbf{x})$ in the region Ω must satisfy the equations of steady motion and continuity and the defining relation

$$\rho(\mathbf{U} - \mathbf{U}_0)\nabla\mathbf{U} = \nabla P \qquad (\mathbf{U}_0 = (U_0, 0)),$$
$$\rho \operatorname{div} \mathbf{U} = (\mathbf{U}_0 - \mathbf{U})\nabla\rho, \; dP/d\rho = c^2 \quad (P(\theta_0) = P_{00}).$$

The boundary conditions which correspond to the physical conditions on the external surface of the layer, the rigid wall, and which follow from the laws of conservation on the front, have the form

$$P = P_0(x) \; (P_0(x) \to P_1 < \infty, \; x \to \infty) \text{ for } y = h,$$
$$V = 0 \text{ for } y = 0,$$
$$P = \rho_0 |\mathbf{U}|^2/\theta, \quad \mathbf{U} = \theta U_0 (1 + s'^2)^{-1}(1, -s'),$$
$$dP/d\rho = c^2 \quad (P(\theta_0) = P_{00}) \text{ for } x = s(y).$$

Here, when deriving the second condition on the front we used the kinematic relation $\mathbf{D} = -U_0(\nabla F/|\nabla F|^2)(\partial F/\partial x)$, where $\mathbf{D}$ is the wave velocity, and $F = x - s(y) \equiv 0$ is the equation of the front in explicit form; the prime denotes differentiation with respect to y. The unknown function $s(y)$ must satisfy the boundary conditions which follow from the choice of the system of coordinates and from the consistency of the boundary conditions

$$s'(0) = 0, \quad s = 0, \quad s' = (\rho_0\theta_0 U_0^2/P_{00} - 1)^{1/2} \quad (y = h).$$

By changing to the dimensionless variables

$$P = \rho_0\theta_0 U_0^2 p, \quad \mathbf{U} = \theta_0 U_0 \mathbf{u}, \quad \mathbf{u} = (u, v), \quad \Delta = \theta/\theta_0$$

(x and s are normalized with respect to h without change in notation) and after making certain transformations, the equations and conditions of the problem can be rewritten in the form

$$(1 - \theta_0 u)u_x - \theta_0 v u_y = (1 - \theta)p_x, \tag{2.1}$$
$$(1 - \theta_0 u)v_x - \theta_0 v v_y = (1 - \theta)p_y,$$
$$u_x + v_y = (\varkappa^2 - 1)[(\theta_0 u - 1)p_x + \theta_0 v p_y],$$
$$d\Delta/dp = 1 - \varkappa^2 \quad (p(1) = p_{00}, \quad \varkappa^2 = 1 - U_0^2/c^2) \quad \mathbf{x} \in \Omega;$$
$$p = p_0(x) \; (p_0(x) \to p_1, \; x \to \infty) \text{ for } y = 1; \tag{2.2}$$
$$v = 0 \text{ for } y = 0; \tag{2.3}$$

$$p = u = \Delta/(1 + s'^2) = p_*(y),$$
$$v = -s'p_*,\ d\Delta/dp = 1 - \varkappa^2\ (p(1) = p_{00})\ \text{for}\ x = s(y),$$
$$s'(0) = 0;\quad s = 0,\quad s' = \sqrt{p_{00}^{-1} - 1} = b\quad (y = 1). \tag{2.4}$$

Here the letter subscript denotes partial differentiation.

We will confine our consideration to the case when $\theta \ll 1$ (and the porosity and deformation of the matrix are small). Neglecting the small terms in Eqs. (2.1) we obtain a system of equations of the form

$$u_x = p_x,\ v_x = p_y,\ \varkappa^2 p_x = -v_y. \tag{2.5}$$

From the first equation of (2.5) and the first condition of (2.4) we have $u(x) = p(x)$. Eliminating u from (2.5), we obtain the equation

$$\varkappa^2 p_{xx} + p_{yy} = 0. \tag{2.6}$$

We will eliminate u, v and Δ from the boundary conditions. Putting $\Delta = 1 + \varepsilon$, the equation of state can be written in the form

$$p = p_{00} + K\varepsilon\quad (K = (1 - \varkappa^2)^{-1}).$$

Eliminating ε from conditions (2.4) we obtain

$$p = p_*(y) = \frac{K - p_{00}}{K(1 + s'^2) - 1}.$$

We will differentiate this relation and the condition $v = -s'p_*$ along the front with respect to y

$$p_y + s'p_x = p_*',\quad v_y + s'v_x = -(s''p_* + s'p_*').$$

We will add to these the equations from system (2.5), which in the limit also hold on the front, and we will solve the system obtained for p_x, p_y, v_x, and v_y. Problem (2.1)-(2.4) then reduces to determining the function $p(x)$, harmonic in the region $\Omega_1^+(x_1, y) = \Omega(\varkappa x_1, y)$ $(x_1 = x/\varkappa)$, and the function $s(y)$ from the conditions

$$p_y = 0\ (y = 0),\ p = p_0(\varkappa x_1)\ (y = 1); \tag{2.7}$$

$$\frac{\partial p}{\partial x_1} = \frac{\varkappa(s''p_* + 2s'p_*')}{s'^2 + \varkappa^2},\quad \frac{\partial p}{\partial y} = \frac{(\varkappa^2 - s'^2)p_*' - s's''p_*}{s'^2 + \varkappa^2}\ (x = s(y)), \tag{2.8}$$

$$(p_*' = 2s's''\dot{p}_*,\quad \dot{p}_* = dp_*/d(s'^2) = K(p_{00} - 1)[K(1 + s'^2) - 1]^{-2});$$

$$s'(0) = 0;\quad s = 0,\quad s' = b,\quad s'' = \frac{a(b^2 + \varkappa^2)}{p_{00}(1 - 4b^2K)}\ (y = 1). \tag{2.9}$$

Here $a = dp_0/dx|_{x=0}$, and the condition for $s''(1)$ follows from the condition of continuity of $\partial p/\partial x_1$ at the point $x_1 = 0$, $y = 1$.

Hence, there is a single condition on the known parts of the boundary of the region Ω_1^+ and two conditions on the unknown parts. Note that if Eq. (2.6) is asymptotically accurate with respect to θ, the conditions (2.7) and (2.8) are accurate.

3. The Functional Equation of the Problem. We will introduce the complex variable $z = x_1 + iy$ and the function $\Phi(z) = \partial p/\partial x_1 - i\partial p/\partial y$, which is analytical in $\Omega_1 = \Omega_1^+ \cup \Omega_1^-$, where Ω_1^- is the region symmetrical to the region Ω_1^+ with respect to the x_1 axis (Fig. 3a); the condition $\Phi(z) = \overline{\Phi}(\overline{z})$ is satisfied.

In the curvilinear part of the boundary the real and imaginary parts of the functions $\Phi(z)$ are connected with the equation of this boundary by the nonlinear differential relations (2.8). When $y = \pm 1$ its real part $\partial p/\partial x_1 = \varkappa(dp_0/dx)_{x=\varkappa x_1}$ is specified.

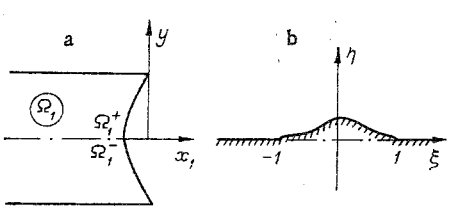

Fig. 3

We will write the necessary and sufficient condition for the complex-valued function of the points of the boundary to be extended into the depth of the region. One of these conditions is that the Cauchy-type integral should vanish at any point outside the region [2]. Since the Cauchy-type integral is an analytical function, it is sufficient for it to vanish off any arc which lies as a whole outside Ω_1, e.g., on a section of the real axis

$$I = \frac{1}{2\pi i}\int_L \frac{\Phi_L dz}{z - x_0} = 0, \quad X_1 \leqslant x_0 \leqslant X_2 \quad (X_1 > s(0)/\varkappa),$$

where $L = L_1 \cup L_2$; $L_1 = \{x_1 < 0, y = \pm 1\}$; $L_2 = \{x_1 = \varkappa^{-1}s(y), -1 \leq y \leq 1\}$; Φ_L is the boundary value of Φ.

We will transform the integrals with respect to L_1 and L_2 using the Cauchy–Riemann formula, conditions (2.7), and the properties of symmetry. We finally obtain

$$I[x_2; s(y)] = I_1 + I_2,$$
$$I_1 = \int_{L_1} = \frac{1}{\pi}\int_{-\infty}^{0} \frac{\varkappa^2 dp_0/dx + (\partial p/\partial y)_{y=1}}{(x - x_2)^2 + \varkappa^2} dx, \tag{3.1}$$
$$I_2 = \int_{L_2} = \frac{1}{\pi}\int_0^1 \frac{s''(s - x_2)\, p_* + [(s - x_2)\, s' - \varkappa^2 y]\, p'_*}{(s - x_2)^2 + \varkappa^2 y} dy$$
$$(X_3 \leqslant x_2 \leqslant X_4,\ s(0) < X_3 < X_4).$$

Equation (3.1) is the basic functional equation of the problem which serves to determine $s(y)$. After $s(y)$ is obtained, the field of arbitrary p can be calculated using the Cauchy integral. A similar condition has been proposed for the approximate solution of linear problems in [3] and has been realized in [4].

The integral I_1 contains the boundary value of the function p_y on L_1. We will further establish a relationship between $p_y(x, 1)$ and $s(y)$. With this aim we will transform the region Ω_1. The function $\zeta = \xi + i\eta = -i \sinh(\pi/2)z$ transfers Ω_1 into the upper half-plane ζ with a cutout "lune" (the region Ω_2 in Fig. 3b). In this case the rays $z = x_1 \pm i$ are converted into the rays $\zeta = \xi = \pm \cosh(\pi/2)x_1$, and the section $\{x_1 = 0, -1 \leq y \leq 1\}$ is converted into the section $\{-1 \leq \xi \leq 1, \eta = 0\}$.

On the boundary $\partial\Omega_2$ of the region Ω_2 the following integral relation holds:

$$\Phi[z(\zeta_0)] = \frac{1}{\pi i}\int_{\partial\Omega_2} \frac{\Phi d\zeta}{\zeta - \zeta_0} \quad (\zeta_0 \in \partial\Omega_2).$$

Hence

$$\frac{\partial p}{\partial y}\Big|_{\zeta = \xi_0} = \frac{1}{\pi}\int_{\partial\Omega_2} \mathrm{Re}\frac{\Phi d\zeta}{\zeta - \xi_0} \quad (\xi_0 > 1). \tag{3.2}$$

On the right side of (3.2) p_y for $\xi_0 > 1$ and $\xi_0 < -1$ does not appear explicitly, so that (3.2) solves the problem of determining $p_y(x, 1)$ for specified $s(y)$.

The integral over $\partial\Omega_2$ can be divided into parts

$$\int_{\partial\Omega_2} = J_1 + J_2, \quad J_1 = \int_{-\infty}^{-1} + \int_1^{\infty}, \quad J_2 = \int_{-1}^{1}.$$

We will now integrate in the plane Ω. As a result of transformations, connected, in particular, with the separation of the singularity in the function under the integral and the replacement $x = 1 - t^{-1}$ in J_1, we obtain for J_1 and J_2 the following final expressions which are convenient for calculations:

$$p_y(x, 1) = J_1 + J_2,$$
$$J_1[t(x)] = \xi(t)\left\{\int_0^1 \frac{G(t, t_0) - G_0(t)}{t - t_0} dt_0 - G_0(t)\ln\frac{1 - t}{t}\right\},$$
$$G = \frac{dp_0}{dx}\Big|_{x = x(t_0)} \frac{(t_0 - t)\sinh[\pi x(t_0)/2\varkappa]}{\xi^2(t_0) - \xi^2(t)}, \quad G_0 = \frac{dp_0}{dx}\Big|_{x = x(t)} \frac{\varkappa}{\pi\xi(t)}, \tag{3.3}$$
$$\xi(t) = \mathrm{ch}\,[\pi x(t)/2\varkappa], \quad x(t) = 1 - t^{-1},$$
$$J_2[\xi(x)] = \frac{1}{2}\int_0^1 \left\{\frac{Ap'_* + Bg}{|\zeta_0 - \xi|} + \frac{(A_1 - A_2)\, p'_* + (B_2 - B_1)\, g}{|\zeta_0 + \xi|}\right\} dy,$$
$$A = A_1 + A_2, \quad B = B_1 + B_2, \quad \eta_0 = -\sinh\frac{\pi s}{2\varkappa}\cos\frac{\pi}{2}y,$$

$$A_1 = -\xi_0 \operatorname{sh}\frac{\pi s}{2\varkappa}\sin\frac{\pi}{2}y, \quad A_2 = \frac{1}{2}\operatorname{sh}\frac{\pi s}{\varkappa}.$$
$$B_1 = -\xi_0 \operatorname{ch}\frac{\pi s}{2\varkappa}\cos\frac{\pi}{2}y, \quad B_2 = \frac{1}{2}\sin\pi y. \tag{3.3}$$
$$|\zeta_0 \pm \xi| = (\xi_0 \pm \xi)^2 + \eta_0^2, \quad \xi_0 = \operatorname{ch}\frac{\pi s}{2\varkappa}\sin\frac{\pi}{2}y.$$
$$\xi = \operatorname{ch}\frac{\pi x}{2\varkappa}, \quad g = \varkappa^{-1}(s''p_* + s'p_*').$$

4. A Method for the Numerical Solution of the Fundamental Equation of the Problem and the Results of Calculations. We write the functional

$$H(s) = \int_{X_3}^{X_4} |I(x_2; s)|\, dx_2,$$

defined on the set of functions S, twice continuously differentiable and satisfying the conditions (2.9) at the ends of the section [0, 1].

H(s) reaches a minimum of zero on the functions–solutions (numerical calculations confirm the uniqueness of the solution).

We will seek a minimum of H(s) by the method of trial and error on subsets of the functions $S_n \subset S$, where S_n are sets of cubic spline-functions [5], and n is the number of divisions of the section [0, 1]. As a first approximation we will take n = 2 and we will confine ourselves to the case when n = 3 for the numerical solution of the problem with acceptable accuracy. For each approximation $s_n \in S_n$ the values of I will be calculated from Eqs. (3.1), and the values of $p_y(x, 1)$ will be calculated from Eqs. (3.3), which are obtained on the assumption that s is the true solution. We will assume that $p_y(x, 1)$ calculated in this way converges to the accurate solution as $s_n \to s$ (uniformly).

In fact, the computational procedure consists in finding a minimum of a function of n − 1 variables, which are the instants $M_i = s_n''(y_i)$ at intermediate nodes. Calculation on a grid M_2, M_3 (n = 3) with a small step showed that the surface $H(M_2, M_3)$ belongs to the "ravine" type, and the direction of the "bottom of the ravine" coincides approximately with the direction of the straight line $M_2 + M_3 = \text{const}$. Correspondingly, we used a modified method of searching for the minimum of the "ravine" type function in the program [6].

We will now consider the mathematical nature of the problem and the fundamental equation to which it can be reduced. Problems with unknown boundaries belong to the class of inverse problems, the usual methods of solving which often lead to instabilities. The same can also be said of Eq. (3.1), since it is an abstract Fredholm equation of the first kind. The problem can be reduced to solving an operator equation of the second kind, but the numerical realization of the solution of (3.1) gives rise to less doubts. Unlike [7], where a similar method leads to a stable computational algorithm, the conditions in the boundary value problem presented here are not of the same type. Calculations show that in certain versions the values of the functional reach a secondary minimum and the solution does not satisfy the condition of continuity of $p_y(x, 1)$ at the point x = 0; the variation of δs_3 causes a variation in δp_y according to Eqs. (3.2), which compensates for the effect of δs_3 in the integral I. For regularization purposes a term is added to the functional representing the discrepancy in satisfying the boundary condition for $p_y(x, 1)$ [8]. Note that for the same reason the equation I = 0 is written in terms of Φ (as in [7]), and not in terms of the analytical function $p - iv/\varkappa$ (which would be somewhat simpler). We would expect the functional H in this version to be more sensitive to s(y).

The error of the solution can be estimated from the quantity $\delta = (H_m / H_1) \cdot 100\%$, where H_m is the value of the minimum of H achieved, and $H_1 = \int_{X_5}^{X_6} |I|\, dx_2$, a $[X_5, X_6]$ is the section of the x axis symmetrical to the section $[X_3, X_4]$ with respect to the point A at which $I = \Phi = \partial p/\partial x_1$. It was formed here from these considerations. Since the solution in the region is found using the Cauchy integral it accurately satisfies the equations inside the region. It follows from the Sokhotskii equation for the limiting values of an integral of the Cauchy type $\Phi - \Phi^- = \Phi_L$, where Φ^- is the limiting value of a Cauchy-type integral outside the region Ω_1, that the quantity $\delta_0 = |\Phi^-/\Phi_L| \cdot 100\%$ represents the discrepancy in satisfying the boundary conditions, since in the accurate solution $\Phi^- = 0$. The point A can be taken as the most representative, since the solution in the neighborhood of the foot of the front varies strongly. For practical calculations it is more convenient to take δ, representing the ratio not of the limiting but of the average values of $|\Phi|$ on the right and left of the front of the front. It is clear intuitively that the values of δ must be close to δ_0.

The accuracy achieve is also confirmed by: a) The branch of the function $p_y(x, 1)$ reaches a boundary

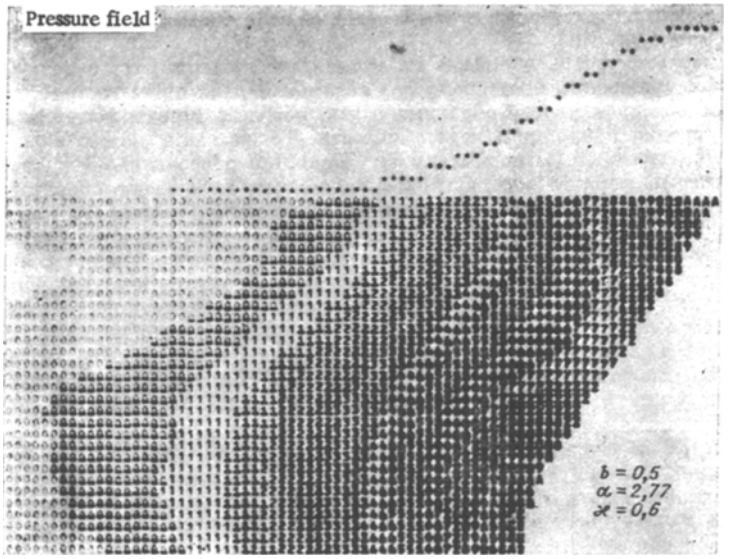

Fig. 4

value when x = 0, and b) the values of p reach an asymptotic $p \to p_1$ when $x \to -\infty$ as a result of integration of the field over the front in the depth of the region. Calculations show that the accuracy of a) and b) correspond to the estimate δ. The values of δ attained are $\approx 0.5\%$, and the asymptotic b) is reached with relative accuracy not exceeding 2.5%.

To interpolate s(y) in the second approximation we used the spline-function $s_3(y)$ on a nonuniform grid. For the majority of versions the length of the intervals were chosen in order to improve the estimate δ from several percent to $\approx 0.5\%$. When debugging the program we chose the optimum values of the internal parameters of the problem (the number of points, the iteration steps, etc.).

Figure 4 shows an example of the numerical calculation of the pressure field (the components of the vector of the mass velocity u), normalized to p_{00} in the physical plane and in the symbolic form of writing. The number of splittings over the thickness of the layer is 30. A change to the next symbol indicates a change of p/p_{00} by 0.05. The numbers 0, $\underline{0}$, 1, $\underline{1}$, 2, $\underline{2}$, ... indicate zones of reduced pressure, and the letters A, $\underline{A}$, B, $\underline{B}$, C, $\underline{C}$, ... indicate the zones of increased pressures, so that the symbol A corresponds to $p/p_{00} = 1 \pm \varepsilon_0$, $\underline{A}$) $1.05 \pm \varepsilon_0$, B) $1.1 \pm \varepsilon_0, \ldots$, $\underline{9} = 0.95 \pm \varepsilon_0$, $9 = 0.9 \pm \varepsilon_0, \ldots$ $0 = \pm\varepsilon_0$ ($\varepsilon_0 = 0.025$).

The graph of the loads is shown by the asterisks. The first row of the upper symbols also relates to the load. The pressure on the surface was specified in the form

$$p_0(x) = p_{00} \exp\left[(-1)^{j+1}\alpha x^j\right] \quad (j = 1, 2).$$

Hence, we varied four external parameters of the problem: α, the j-characteristics of the pulse length and shape, $b = s'(1) = (U_0^2/D_0^2 - 1)^{1/2} = \tan\beta$ – its intensity or angle of inclination of the front at the point B (see Fig. 1), and $\varkappa = (1 - U_0^2/c^2)^{1/2}$. When choosing b and $\varkappa$ we took into account the following facts. First, p_{max}, the maximum pressure attained at the point A, should not be high (otherwise the assumptions made may break down). We can calculate

$$p_{max}/p_{00} = (b^2 + \varkappa^2)/\varkappa^2,$$

and we assumed $p_{max}/p_{00} < 5$. Secondly, the denominator in the expression for $s''(1)$ in (2.9) when $\varkappa^2 = 3b^2$ vanishes, and when $\varkappa^2 > 3b^2$ the sign of $s''(1)$ becomes unnatural: A falling load corresponds to an increase in the intensity of the shockwave into the depth of the region. In [8] to explain this situation an investigation was made on an example of the problem of small stationary perturbations of an inclined shockwave propagating in half-space. It was established that for $\varkappa^2 \geq 3b^2$ the solution has an integrated singularity at the point B (an indirect indication of the instability of the solution). When $\varkappa^2 < 3b^2$ it is everywhere continuous in $\Omega \cup L$. Physically, the condition $\varkappa^2 < 3b^2$ means that the isobars approach from above, $\varkappa^2 = 3b^2$ horizontally, and $\varkappa^2 > 3b^2$ from below, to the front of the inclined shock wave. When $D_0 < U_0 < c$ there are regions (not of zero measure) of the parameters, which satisfy the inequality in some sense. It can be seen that small angles $\beta (0 \leq \tan\beta \leq \varkappa/\sqrt{3})$ correspond to the inequality $\varkappa^2 \geq 3b^2$.

TABLE 1

No. of figure	No. of curve	b	$\varkappa$	l	j	e	s(0)
5	1	0,25	0,30	∞			0,13
	2	0,25	0,30	0,25	2	0,25	0,27
	3	0,50	0,60	∞			0,26
	4	0,50	0,30	∞			0,36
	5	0,50	0,60	0,50	2	0,28	0,56
	6	0,50	0,30	0,50	2	0,10	0,45
	7	1,00	0,60	∞			0,70
	8	1,00	0,60	1,00	1	0,22	0,93
	9	1,00	0,90	1,00	1	0,39	1,10
6	1	0,50	0,60	∞			0,26
	2	0,25	0,30	∞			0,13
	3	0,50	0,60	0,50	1	0,53	0,53
	4	0,25	0,30	0,50	1	0,20	0,20
	5	0,25	0,30	0,25	1	0,29	0,29

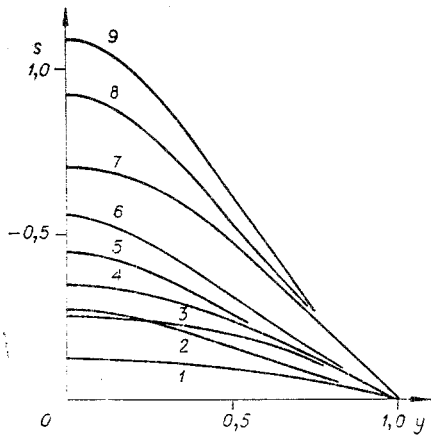

Fig. 5

Calculations were made for values of b = 1.0, 0.5, and 0.25, and $\varkappa$ = 0.9, 0.6, (b = 1), $\varkappa$ = 0.6, 0.3 (b = 0.5), $\varkappa$ = 0.3 (b = 0.25). In this case $\varkappa$ = 0.9 corresponds to $U_0 \approx 0.45c$, $\varkappa = 0.6$ – $U_0 \approx 0.8c$, $\varkappa = 0.3$ – $U_0 \approx 0.954c$.

We will use the characteristic length of the pulse of value $l = -x_0$ (x_0 is the coordinate where the intensity of the load falls by half). In the calculations we used $l = \infty$, 1.5; 1.0; 0.5; 0.25 (j = 1); l = 1.0; 0.5; 0.25 (j = 1) (corresponding to α = 0; 0.31; 0.7; 2.77; 11.4 (j = 2); α = 0.7; 1.39; 2.77 (j = 1)).

The isobars are concentrated around the point A, and for long loading pulses ("steps" in particular) have the shape of arcs of ovals stretched upwards. As the parameter $\varkappa$ is reduced the picture, as it were, contracts along the x axis, although the change in the position of the front is relatively small. The slopes of the isobars approaching the front are in complete agreement with the results of the linear theory [8].

In the particles after the transmission of a shock wave and at times in a part of the front of considerable thickness additional loading occurs and may be tens of percent of the pressure on the front. The idea of unloading behind the front was a priori.

For $l \sim 1$ the isobar picture is complicated by the effect of unloading on the external surface. A region of reduced pressure appears on the front. The slope of the front changes sign when there is attenuation.

We will represent the attenuation by the quantity $e = 1 - p_{min}/p_{00}$

$$\left(p_{min} = \min_{0 \leqslant y \leqslant 1} p_*(y)\right).$$

The effect of attenuation is reduced considerably when the angle β is reduced. The same value of e is obtained when changing from b = 0.5 to b = 0.25 ($\varkappa$ = 0.3) by reducing the pulse length by approximately a half. This can be explained by the fact that as $\beta \to 0$ the front and the isobars become almost vertical, while the wave is plane.

The shape of the pulse has less effect on the solution than its length. When l is halved the value of e

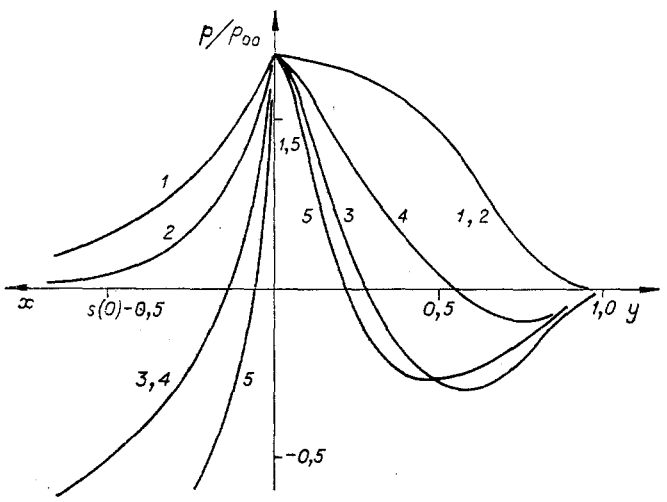

Fig. 6

doubles. Comparing the results for different pulse shapes (j = 1, 2) in the two situations: b = 0.5, $\varkappa$ = 0.6, l = 0.5 and b = 0.25, $\varkappa$ = 0.3, l = 0.25, we obtain approximately the same value of the attenuation (about 0.27). For other values of b and $\varkappa$ the effect of the shape is greater: e ≈ 0.39 (b = 1, j = 1, $\varkappa$ = 0.9), e ≈ 0.18 (b = 1, j = 2, $\varkappa$ = 0.9).

As the velocity of sound increases (as $\varkappa$ increases) the value of e increases considerably. By comparing the solutions for b = 1, l = 1, j = 1 and different $\varkappa$, we obtain e ≈ 0.39 ($\varkappa$ = 0.9), e ≈ 0.22 ($\varkappa$ = 0.6). The same correspondence is observed for b = 0.5 and different $\varkappa$.

Figures 5 and 6 show lines of the fronts and the pressure distribution along the fronts and the rigid wall. The relationship between the parameters and the numbers on the figures is given in the table, where we also show values of e and s(0).

Curves 1 and 2 (Fig. 6) for $p_*(y)/p_{00}$ coincide, which indicates, first, partial similarity (in those cases the curves of $p(x, 0)/p_{00}$ diverge) in the case of step loading and the same values of $p_{max}/p_{00} = (b^2 + \varkappa^2)/\varkappa^2$; and, second, indirectly regarding the accuracy attained: The estimate of the relative difference of $p_*(y)$ (with respect to p_{max}) in a uniform metric does not exceed 2%. If the pulse is not a "step," similarity is not observed (compare curves 3 and 4 in Fig. 6).

For short loading pulses (l = 0.25) a short wave is formed in the neighborhood of point A: very high gradients ($\partial p/\partial x \sim 10^2$) for maximum values of the functions themselves. We will analyze the effect of the neglected terms in system (2.1). Direct calculations using the data from the calculations show that the terms $\theta_0 v u_y$ and $\theta_0 v v_y$ up to $\theta_0 \approx 0.3$ remain an order of magnitude less than $|\nabla p|$. In addition, the coefficients $(1 - \theta_0 u)/(1 - \theta) \approx 1 - (1 - p_{00})\theta_0$ in the first two and $(1 - u\theta_0)$ in the third of Eqs. (2.1) are replaced by unity. The latter may introduce the greatest error. However, the values of the functions at the point A are calculated accurately here, while the neighborhood, where u = p may considerably exceed unity, is small, so that we would expect that consideration of the convective terms when $\theta < 0.2$ has a small effect on the solution as a whole unlike [9], where the situation is basically different.

LITERATURE CITED

1. V. Herman, "The defining equation for dynamic compression of plastic porous materials," Sb. Per. Mekhanika, No. 5 (1970).
2. M. A. Lavrent'ev and B. V. Shabat, Methods of the Theory of Functions of a Complex Variable [in Russian], Fizmatgiz, Moscow (1958).
3. V. D. Kupradze, "Approximate solution of problems of mathematical physics," Usp. Mat. Nauk, 22, No. 2 (1967).
4. Yu. V. Vereyuzhskii, A. I. Vusatyuk, and V. V. Savitskii, "Numerical realization of V. D. Kupradze's method for solving certain static problems in the theory of elasticity," in: The Resistance of Materials and the Theory of Structures [in Russian], Republic Interdepartmental Scientific Collection, Budivel'nik, Kiev, No. 25 (1975).
5. S. B. Stechkin and Yu. N. Subbotin, Splines in Computational Mathematics [in Russian], Nauka, Moscow (1976).

6. A. A. Pervozvanskii, Search [in Russian], Nauka, Moscow (1970).
7. I. V. Simonov, "Diffraction of a plane shock wave by corners in an ideally packed medium," Izv. Akad. Nauk SSSR, Mekh. Tverd. Tela., No. 1 (1978).
8. I. V. Simonov, "Numerical-analytical investigation of the problem of a load traveling in a layer of ideally packed material," Preprint Inst. Probl. Mekh. Akad. Nauk SSSR, No. 115 (1978).
9. A. A. Grib, O. S. Ryzhov, and S. A. Khristianovich, "The theory of short waves," Zh. Prikl. Mekh. Tekh. Fiz., No. 1 (1960).

DYNAMICS OF THE FRACTURE OF UNIDIRECTIONAL GLASS – PLASTIC

M. V. Stepanenko

UDC 539.3+539.4

The dynamic problem of the concentration of stresses and the subsequent propagation of a flaking crack in unidirectional glass–plastic is considered. A plane deformation is investigated and the glass–plastic material corresponds to the model considered in [1], i.e., it is assumed that the armoring of the fiber is in the uniaxial stressed state (extension–compression), and the filler (binding) is subjected only to a shear stress.

For practical purposes it is important to explain the features of the kinetics of cracks and the possibility of localizing them. In this paper we solve these problems by a numerical method, which enables us, with acceptable accuracy, to describe the nonstationary wave process of stress concentration and subsequent fracture.

The problem of the dynamic concentration of stresses in the region of a defect in a glass–plastic is considered in a limited number of papers (see, e.g., [2, 3]). Here we use the formulation of the problem given in [2], where the solution of the dynamic problem is obtained in the form of the sum of a series with a finite number of terms, each of which corresponds to the contribution of a wave reflected from a certain fiber. In [3] the problem of approximating the dynamic solution to the static solution with time is discussed. It is not possible to analyze the kinetics of fracture using analytical methods.

The formulation of the problem is as follows: A fiber is stretched to infinity with a constant force; at zero instant of time, due to a certain defect, one of the fibers instantaneously fractures; then the broken fiber begins to be unloaded, while the load on all the others is increased, the perturbations from one rod to another being transferred by shear waves into the binder; if we assume that the increase in the load on all the fibers does not lead to their fracture, fracture can only occur in the form of longitudinal flaking cracks.

We will direct the y coordinate along the fiber, and the x coordinate perpendicular to it, and we will take the origin of coordinates at the defect. We will take as the unit of measurement the quantities which relate to the filler: the density ρ, the shear modulus G, the velocity of shear waves $c_2 = \sqrt{G/\rho}$, and the distance between fibers H (H/c_2 is the unit of time). We will introduce the following notation: ρ_1, E, and h are the density, Young's modulus, the thickness of the fiber ($c_1 = \sqrt{E/\rho_1}$ is the velocity of sound in the fiber), $u_j(y, t)$ is the displacement of the j-th fiber ($j = 0, \pm 1, \pm 2, \ldots$), $v(x, y, t)$ is the displacement of a point of the filler, $\sigma_j = E\partial u_j/\partial y$, $\tau = G\partial v/\partial x$ are the stresses in the fibers and the binder.

The glass–plastic is stretched to infinity with a stress P. We will solve the problem with respect to additional perturbations due to breaking of the fiber (suppose this is the fiber $j = 0$). The equations in the displacements and the boundary conditions have the form (the initial conditions are the zero conditions)

$$\partial^2 v/\partial t^2 = \partial^2 v/\partial x^2; \tag{1}$$

$$\frac{1}{c_1^2}\frac{\partial^2 u_j}{\partial t^2} = \frac{\partial^2 u_j}{\partial y^2} + \frac{1}{Eh} Q_j, \quad Q_j = \tau|_{x=j+0} - \tau|_{x=j-0}; \tag{2}$$

$$v(j, y, t) = u_j(y, t); \tag{3}$$

$$\partial u_j/\partial t = -P/E \ (j = 0), \ u_j = 0 \ (j \neq 0) \text{ for } y = 0, \tag{4}$$

Novosibirsk. Translated from Zhurnal Prikladnoi Mekhaniki i Tekhnicheskoi Fiziki, No. 4, pp. 155–163, July–August, 1979. Original article submitted May 30, 1978.

0021-8944/79/2004-0513$07.50